

Article

Cobalt-Copper Oxide Catalysts for VOC Abatement: Effect of Co:Cu Ratio on Performance in Ethanol Oxidation

Květa Kupková¹, Pavel Topka² , Jana Balabánová², Martin Koštejn², Květuše Jiráťová², Jean-Marc Giraudon³, Jean-Francois Lamonier³ , Jaroslav Maixner⁴ and František Kovanda^{1,*}

¹ Department of Solid State Chemistry, University of Chemistry and Technology, Technická 5, 166 28 Prague, Czech Republic

² Institute of Chemical Process Fundamentals of the Czech Academy of Sciences, Rozvojová 135, 165 02 Prague, Czech Republic

³ Unité de Catalyse et Chimie du Solide, University of Lille, UMR CNRS 8181, Cité Scientifique, CEDEX, 59650 Villeneuve d'Ascq, France

⁴ Central Laboratories, University of Chemistry and Technology, Technická 5, 166 28 Prague, Czech Republic

* Correspondence: frantisek.kovanda@vscht.cz

Abstract: The effect of the Co-Cu oxide catalysts composition on their physicochemical properties and performance in the deep oxidation of ethanol was studied. The catalysts with Co:Cu molar ratios of 4:1, 1:1, and 1:4 were obtained by calcination (4 h at 500 °C in air) of the coprecipitated precursors and characterized in detail using powder XRD, Raman spectroscopy, N₂ physisorption, H₂-TPR, and XPS. The powder XRD and Raman spectroscopy indicated the formation of Co₃O₄ and CuO mixtures rather than Co-Cu mixed oxides. The CuO promoted the Co₃O₄ reduction; the Co-Cu catalysts were reduced more easily than the single-component Co and Cu oxides and the main reduction maxima were shifted to lower temperatures with increasing cobalt content in the catalysts. The Co-Cu oxide catalyst with a Co:Cu molar ratio of 4:1 exhibited the best performance in ethanol gas-phase oxidation, showing the lowest *T*₅₀ (91 °C) and *T*₉₀(CO₂) (159 °C) temperatures needed for 50% ethanol conversion and 90% conversion to CO₂, respectively. The excellent catalytic properties of this Co-Cu oxide catalyst were ascribed to the synergistic effect of Co and Cu components. The high activity and selectivity of the Co-Cu catalyst was attributed to the presence of finely dispersed CuO particles on the surface of Co₃O₄.

Keywords: cobalt-copper oxide catalysts; synergistic effect; ethanol total oxidation; VOC abatement



Citation: Kupková, K.; Topka, P.; Balabánová, J.; Koštejn, M.; Jiráťová, K.; Giraudon, J.-M.; Lamonier, J.-F.; Maixner, J.; Kovanda, F.

Cobalt-Copper Oxide Catalysts for VOC Abatement: Effect of Co:Cu Ratio on Performance in Ethanol Oxidation. *Catalysts* **2023**, *13*, 107. <https://doi.org/10.3390/catal13010107>

Academic Editor: Hongxing Dai

Received: 30 November 2022

Revised: 20 December 2022

Accepted: 23 December 2022

Published: 3 January 2023



Copyright: © 2023 by the authors. Licensee MDPI, Basel, Switzerland. This article is an open access article distributed under the terms and conditions of the Creative Commons Attribution (CC BY) license (<https://creativecommons.org/licenses/by/4.0/>).

1. Introduction

Volatile organic compounds (VOCs) are one of the major contributors to air pollution. They are ozone/smog precursors and efficient greenhouse gases. The VOCs represent environmental and human health risks and, therefore, there is an effort to lower their emissions. The treatment method is chosen according to the composition of VOC-containing off-gas and operational cost of the technology. While thermal oxidation requires temperatures up to 1000 °C, a catalytic oxidizer operates at 250–500 °C depending on the catalyst and the nature of the VOC. This brings energy savings and, therefore, better cost efficiency compared to incineration [1]. Catalysts for VOC oxidation are based on noble metals or transition metal oxides. Noble metal catalysts usually contain palladium, platinum, or rhodium that are expensive and sensitive to poisoning caused by chlorine residue or water vapor [2,3]. On the other hand, transition metal oxides have been found as a cheaper alternative to noble metal catalysts. The oxides of Fe, Ni, Ag, V, Mn, Cu, and Co have shown remarkable catalytic activity.

The Co-Cu oxides already attracted much attention as catalysts for VOC oxidation. Hosseini et al. [4] reported that the Co-Cu oxide exhibited higher activity in 2-propanol oxidation than the Cr-Cu and Mn-Cu oxides due to its higher reducibility and possible

synergistic effect between the Co-Cu mixed oxide and CuO particles. The Co-Cu oxide was also more active in n-hexane oxidation than the Co-Cr or Co ones, either grained or supported on ceria or zirconia [5]. Similarly, the Co-Cu catalyst showed superior activity in CO oxidation due to easier reducibility of the Co-Cu spinels compared to cobalt oxide [6]. The Co-Cu oxide catalyst with a Co:Cu molar ratio of 3:1 supported on alumina exhibited high activity in the simultaneous BTEX and PAH oxidation [7]. Jia et al. [8] found that addition of Co to CuO increased the catalysts activity in oxidation of toluene and ethyl acetate and the catalysts were more active than Co_3O_4 . Lv et al. [9] underlined the importance of surface synergetic oxygen vacancy coupled with the adjacent Cu and Co ions for catalytic activity of the Co-Cu oxides. The cooperative effect of copper and cobalt species was recently confirmed by Carillo et al. [10] in toluene oxidation, with Co:Cu molar ratios of 1:1 and 2:1 showing the highest catalytic activity. The synergistic effect of copper and cobalt oxides on the activity in benzene oxidation was reported by Li et al. [11]. The reducibility of Cu^{2+} species in CuO enhanced with increasing Co content, while the opposite effect was observed for the reducibility of Co with increasing Cu content. The most active catalyst was $\text{Cu}_{0.5}\text{Co}_{2.5}$, which was attributed to its larger surface area, smaller pore size, better reducibility at low temperature, and higher ratio of lattice and adsorption oxygen.

We have shown recently that structured cobalt oxide catalysts can be easily prepared by hydrothermal synthesis under mild conditions [12]. In ethanol oxidation, the performance of catalysts supported on stainless steel meshes was better than that of the pelletized commercial Co_3O_4 , although the cobalt oxide content was nearly 50 times lower [13]. We have demonstrated earlier that mixed oxides (e.g., Co-Mn) may exhibit higher efficiency in ethanol oxidation than the cobalt oxide [14]. Recently, we have shown that Co-Mn mixed oxide catalysts can be supported on stainless steel meshes by magnetron sputtering [15] or hydrothermal synthesis [16]. Moreover, their catalytic activity in ethanol oxidation was 48–114 times higher than that of the commercial pelleted Co-Mn-Al catalyst [16]. In order to investigate the activity of other types of oxides, here we prepared the Co-Cu catalysts by heating of coprecipitated precursors and examined the effect of Co:Cu molar ratio on their physicochemical properties and catalytic performance in the ethanol total oxidation.

2. Results

2.1. Physicochemical Properties of the Catalysts

The Co, Cu, and Na contents in the prepared oxide catalysts are summarized in Table 1. The Co:Cu molar ratios determined from AAS measurements were in good agreement with expected nominal values, which were adjusted in nitrate solutions used for coprecipitation of the precursors. The metal cations content in the oxides was calculated based on their content in the precursors and weight loss during calcination at 500 °C, assuming no loss of metal components occurred during calcination. The catalysts also contained small amounts of sodium cations remaining in the prepared products after washing.

Table 1. Content of Co, Cu, and Na in the prepared Co-Cu oxide catalysts and weight loss determined after 4 h calcination of the dried precursors at 500 °C in air.

Catalyst	Co	Cu (wt.%)	Na	Weight Loss (wt.%)	Co:Cu Molar Ratio
Co	66.3	-	1.75	30.0	1:0
CoCu41	56.7	15.0	0.17	27.1	4:0.98
CoCu11	35.3	37.2	0.34	27.5	1:0.98
CoCu14	14.3	59.3	0.57	24.9	1:3.85
Cu	-	75.1	0.77	22.4	0:1

Powder XRD patterns of washed and dried precursors are shown in Figure 1. The distinct diffraction peaks at 13.9, together with the other peaks at 39.2, 46.5, and 70.6° 2 θ found in powder XRD pattern of the Co-P precursor could be attributed to a phase with

layered hydroxide-like structure, likely a $\text{Co}^{\text{II}}\text{-Co}^{\text{III}}$ layered hydroxide. The CoCu41-P and CoCu11-P precursors were rather amorphous. The Cu-P and CoCu14-P precursors showed diffraction peaks at 19.3 , 27.8 , 40.3 , 41.8 , 46.0 , 63.0 , 66.2 , and 74.9° 2θ , which were ascribed to $\text{Cu}(\text{OH})_2$ (PDF 04-009-4366). The diffraction peaks at 41.8° and 45.4° are coincident with the most intensive diffraction lines of CuO (tenorite), and thus, the presence of a small amount of CuO admixture in these precursors cannot be excluded. A sharp diffraction peak of low intensity at 34.3° 2θ was found in powder XRD pattern of the Cu-P precursor; it was ascribed to sodium nitrate, which was not completely removed by washing.

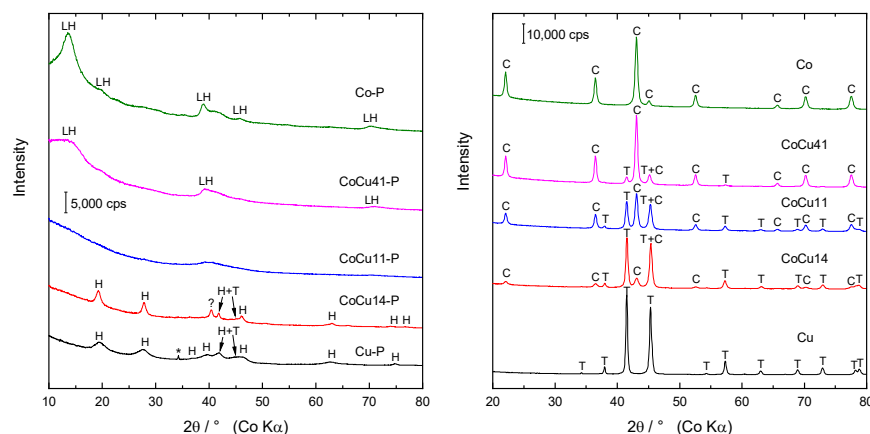


Figure 1. Powder XRD patterns of the coprecipitated precursors (**left**) and oxide catalysts obtained after calcination at 500°C in air (**right**). H— $\text{Cu}(\text{OH})_2$, LH—hydrated layered hydroxide, *— NaNO_3 , ?—unidentified, C— Co_3O_4 , T—CuO (tenorite).

Phase composition of the oxide catalysts obtained after calcination of the coprecipitated precursors at 500°C in air is demonstrated in Figure 1. Powder XRD pattern of the Cu catalyst corresponded to CuO (tenorite, PDF 04-015-5877), with characteristic diffraction lines at 34.2 , 38.0 , 41.5 , 45.3 , 54.3 , 57.3 , 63.0 , 68.9 , 72.9 , 78.2 , and 78.8° 2θ . The Co catalyst contained only Co_3O_4 (PDF 04-005-4386) as a crystalline phase, with the characteristic diffraction lines at 22.1 , 36.5 , 43.1 , 45.1 , 52.6 , 65.7 , 70.2 , and 77.5° 2θ . Powder XRD patterns of the Co-Cu catalysts showed diffraction peaks corresponding to both CuO and Co_3O_4 , the formation of a mixture of spinel-type Co_3O_4 and CuO during calcination of coprecipitated Co-Cu precursors can be expected.

Powder diffraction files provided by the International Centre for Diffraction Data (ICDD PDF-2 database) contain several copper-cobalt mixed oxides with various Co and Cu content from $\text{Cu}_{0.95}\text{Co}_{2.05}\text{O}_4$ (PDF 01-78-2177) to $\text{Cu}_{0.15}\text{Co}_{2.84}\text{O}_4$ (PDF 01-78-2172). These oxides have very similar positions of diffraction lines with only small shifts caused by small difference in the Co and Cu cation sizes. Copper cations are assumed to occupy tetrahedral [6,17] or octahedral positions in the spinel lattice with certain degree of inversion [18]. Therefore, it is difficult to clearly determine from the powder XRD patterns, whether the spinel structure corresponds to Co_3O_4 or $\text{Cu}_x\text{Co}_{3-x}\text{O}_4$ [19]. In mixed Co-Cu spinels, the copper content is represented by x value ranging from 0 to 1 [18]. Values of x calculated for catalysts with Co:Cu molar ratios of 4:1, 1:1, and 1:4 correspond to 0.6, 1.5, and 2.4, respectively. They show excess of copper cations in the CoCu11 and CoCu14 catalysts. La Rosa-Toro et al. [20] suggested that excess of copper cations is segregated at the surface of the catalyst as CuO impurities. This is in line with our observations; the powder XRD patterns showed the presence of CuO in all Co-Cu catalysts. On the other hand, some other authors attributed the diffraction peaks to Co-Cu spinel-like oxides without confronting the similarity with Co_3O_4 peaks [4,19–22] or matched the peaks with Co_3O_4 pattern. Regarding no presence of CuO, they expected incorporation of Cu^{2+} cations into the spinel lattice and suggested formation of a mixed oxide [6,17,23,24]. From the XRD data only, it is difficult to distinguish whether the samples contain Co-Cu mixed oxides with spinel structure, Co_3O_4 or a mixture of Co_3O_4 with a Co-Cu mixed oxide [20,24,25]. In our case, CuO was present

in all Co-Cu catalysts. The quantification of the spinel and CuO contents in the CoCu41, CoCu11, and CoCu14 catalysts was based on the integral intensity of the corresponding diffraction peaks using HighScore Plus software. The evaluated Co₃O₄ to CuO weight ratios were used to calculate corresponding Co:Cu molar ratios (Table 2). In the CoCu41 sample, the Co:Cu molar ratio evaluated from powder XRD data is considerably higher than the expected value (i.e., that adjusted in nitrate solutions used for the precursors synthesis), indicating that less copper was identified by XRD analysis. This finding could be explained by incorporation of copper cations into the spinel lattice or by formation of amorphous copper species, which were not detected by XRD.

Table 2. Crystallite sizes, lattice parameters, and weight ratios of cobalt and copper oxides (Co₃O₄ and CuO) in the catalysts determined from powder XRD data.

Co ₃ O ₄					
Catalyst	Crystallite Size ^a (nm)	Lattice Parameter <i>a</i> (Å)	Co ₃ O ₄ :CuO Weight Ratio	Co:Cu Molar Ratio ^c	Co:Cu Molar Ratio ^d
Co	19	8.084	-	-	-
CoCu41	21	8.090	87:13	4:1	6.6:1
CoCu11	18	8.087	53:47	1:1	1.1:1
CoCu14	13	8.089	16:84	1:4	0.8:4
CuO					
Catalyst	Crystallite Size ^b (nm)	Lattice Parameter			
		<i>a</i> (Å)	<i>b</i> (Å)	<i>c</i> (Å)	β (°)
CoCu41	19	4.695	3.425	5.126	99.341
CoCu11	19	4.690	3.422	5.136	99.532
CoCu14	20	4.688	3.422	5.129	99.565
Cu	30	4.685	3.425	5.130	99.509

^a calculated from the FWHM value of the spinel (311) diffraction line. ^b calculated from the FWHM value of the CuO (−202) diffraction line. ^c nominal (adjusted in nitrate solutions used for the precursors synthesis). ^d determined from powder XRD data.

The crystallite size evaluated from the powder XRD data reflected structure ordering of the studied catalysts. The FWHM (full width in half maximum) values were evaluated from the powder XRD patterns, and the crystallite sizes of spinel-type oxides were calculated as a mean coherence length in [311] direction; the corresponding (311) spinel diffraction line is located around 43.1° 2 θ . The crystallite sizes of CuO were calculated by the same way from the tenorite (−202) diffraction line located around 57.3° 2 θ . The crystallite size of spinel-type oxides in Co, CoCu41, and CoCu11 catalysts was approximately 20 nm; smaller crystallite size of spinel-type oxide (13 nm) was found only for the CoCu14 sample. The CuO crystallite size of about 20 nm was evaluated for all Co-Cu oxide catalysts, whereas the CuO crystallite size of 30 nm was found for the Cu catalyst. The lattice parameters were determined from the cell refinement after the treatment of powder XRD patterns with default profile fitting and matching with appropriate phase (Co₃O₄ and CuO). The spinel lattice parameters in the Co-Cu catalysts were very similar and slightly larger compared to the Co catalyst; however, no significant change in the spinel lattice parameters was observed (Table 2).

Raman spectra of the prepared Co-Cu catalysts are presented in Figure 2. The Co catalyst showed five Raman lines at 192, 477, 518, 616, and 686 cm^{−1}. These lines corresponded to the structural symmetries *F*_{2g}, *E*_g, *F*_{2g}, *F*_{2g}, and *A*_{1g} of the spinel structure. The line positions were in accordance with those reported for Co₃O₄ [26,27]. The most intensive line at 686 cm^{−1} (*A*_{1g}) was associated with octahedral sites vibrations and the *F*_{2g} line at 192 cm^{−1} was attributed to tetrahedral sites [28]. The Cu catalyst showed Raman line at

293 cm^{-1} (attributed to the A_g mode) and two B_g -attributed lines at 344 and 618 cm^{-1} , corresponding to the CuO characteristic lines reported in literature [29,30].

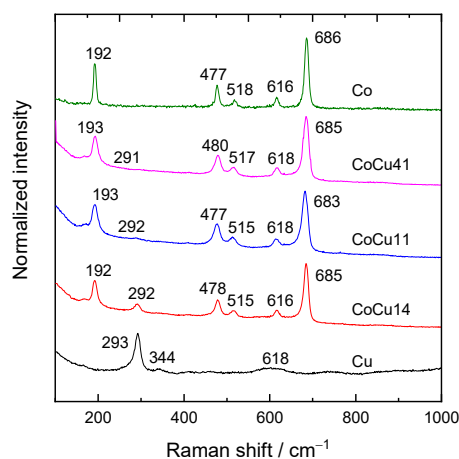


Figure 2. Raman spectra of the examined Co-Cu oxide catalysts.

The Co-Cu catalysts showed Raman lines characteristic for both single oxides, i.e., CuO and Co_3O_4 . Intensity of the strongest CuO line at 293 cm^{-1} decreased with decreasing Cu content in the catalysts. The reported Raman spectra of Co-Cu mixed oxides have shown spectra similar to those of Co_3O_4 with five characteristic lines [31]. A shift in the line positions did not prove clearly the formation of a mixed oxide, as the Raman lines positions depend on the shape and size of crystallites [26,30]. Su et al. [32] observed lines characteristic for Co_3O_4 in Co-Cu mixed oxides; the only difference was the shift from 687 to 664 cm^{-1} and the broadening of this line. Due to the absence of CuO lines in the spectra, the finding was attributed to the formation of Co-Cu spinel. The Raman spectra of the Co-Cu catalysts showed a simple superposition of the individual oxide lines, depending on the various contents of cobalt and copper components in the catalysts (Figure 2). Both powder XRD patterns and Raman spectra of the Co-Cu catalysts indicated that mixtures of Co_3O_4 and CuO rather than Co-Cu mixed oxides were formed after calcination of the coprecipitated precursors.

The isotherms of nitrogen adsorption by catalysts are shown in Figure 3. The measured isotherms were classified as type II isotherms (according to IUPAC) and corresponded to non-porous or macroporous materials [33]. Only a small adsorption (less than 5.5 $\text{cm}^3 \text{g}^{-1}$) at low relative pressures was observed and, therefore, micropores were likely not present in the catalysts.

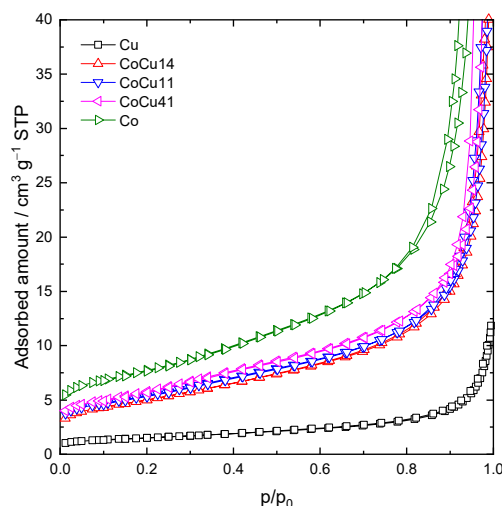


Figure 3. Nitrogen adsorption isotherms of the Co-Cu oxide catalysts.

Table 3 summarizes the textural characteristics, namely surface area S_{BET} , mesopore volume V_{meso} , and average pore diameter d . The Co catalyst showed the largest surface area ($27 \text{ m}^2 \text{ g}^{-1}$), while the Cu catalyst showed the lowest surface area ($5 \text{ m}^2 \text{ g}^{-1}$). The Co-Cu catalysts had a surface area of approximately $20 \text{ m}^2 \text{ g}^{-1}$; the mesopore volume slightly decreased with increasing Cu content in the catalysts. The reported surface area of CuO prepared from precipitated precursors ranged from 2 to $147 \text{ m}^2 \text{ g}^{-1}$ [18,34–36]. Samples with a surface area of about $5\text{--}10 \text{ m}^2 \text{ g}^{-1}$ reported in [20,35,36] were calcined at higher temperatures (at least $400 \text{ }^\circ\text{C}$) for several hours. The heat treatment likely caused sintering of the particles leading to a reduction in surface area. By contrast, some samples treated at higher temperatures showed larger surface area values, likely due to the different precursors used [37].

Table 3. Textural properties of the Co-Cu oxide catalysts determined from nitrogen adsorption (S_{BET} surface area, V_{meso} pore volume of mesopores, d average pore diameter).

Catalyst	S_{BET} ($\text{m}^2 \text{ g}^{-1}$)	V_{meso} ($\text{cm}^3 \text{ g}^{-1}$)	d (nm)
Co	27	0.230	32
CoCu41	21	0.175	32
CoCu11	19	0.089	18
CoCu14	18	0.075	16
Cu	5	0.017	14

Similarly, the surface area of bulk Co_3O_4 obtained from precipitated precursors is reported to range from 6 to $78 \text{ m}^2 \text{ g}^{-1}$ [38,39]. Surface area of the Co catalyst was comparable with that reported by other authors using nitrate solutions and sodium carbonate as precipitant [40–43]. Other authors reported similar surface area of Co_3O_4 prepared from precursors precipitated by sodium hydroxide [40], ammonia [43], and ammonium carbonate solutions [43]. Li et al. [17] prepared the Co-Cu mixed oxide using nitrates as source of metal cations and sodium carbonate as a precipitant. The surface area of the mixed oxide samples ranged from 43 to $100 \text{ m}^2 \text{ g}^{-1}$, while the Co_3O_4 sample showed a surface area of $52 \text{ m}^2 \text{ g}^{-1}$; the precursors were thermally treated under mild conditions (at $350 \text{ }^\circ\text{C}$ for 5 h).

The reduction properties of the catalysts were examined using H_2 -temperature programmed reduction. The measured reduction profiles are shown in Figure 4 and the hydrogen consumptions are summarized in Table 4. The Co catalyst exhibited two reduction peaks: a smaller peak with a maximum at $292 \text{ }^\circ\text{C}$ and a larger peak with a maximum at $378 \text{ }^\circ\text{C}$. Only Co_3O_4 was found in the powder XRD pattern of the Co catalyst. Its reduction profile was similar to the reported reduction profiles of Co_3O_4 species with more or less significant overlap of the two peaks mentioned above [6,10,19,26,44]. The first reduction peak can be attributed to the reduction of Co^{3+} to Co^{2+} , while the other one at higher temperature corresponds to the reduction of Co^{2+} to Co^0 . The reduction profile of the Cu catalyst was rather complex with a broad reduction feature ranging from 200 to $450 \text{ }^\circ\text{C}$ with maximum at $414 \text{ }^\circ\text{C}$. The powder XRD revealed the presence of CuO in this catalyst. Thus, this reduction feature might be ascribed to the reduction of Cu^{2+} species to metallic copper. This assumption was confirmed by total hydrogen consumption of the Cu catalyst, which corresponded to the reduction of CuO to Cu (Table 4). Different H_2 -TPR profiles of CuO were reported in literature, consisting of a single reduction peak [4,6,10] or several reduction peaks [18,19]. This inconsistency may be ascribed to different CuO particle size (dispersed CuO, small crystallites, or bulk CuO), which leads to different Cu^{2+} and Cu^+ reduction temperatures [26,45]. The Co-Cu catalysts were reduced at lower temperatures compared to the Co and Cu samples (Figure 4, Table 4). The main reduction maxima were shifted to lower temperatures with increasing cobalt content in the catalysts; T_{max} of 313, 271, and $253 \text{ }^\circ\text{C}$ were found for the CoCu14, CoCu11, and CoCu41 catalysts, respectively.

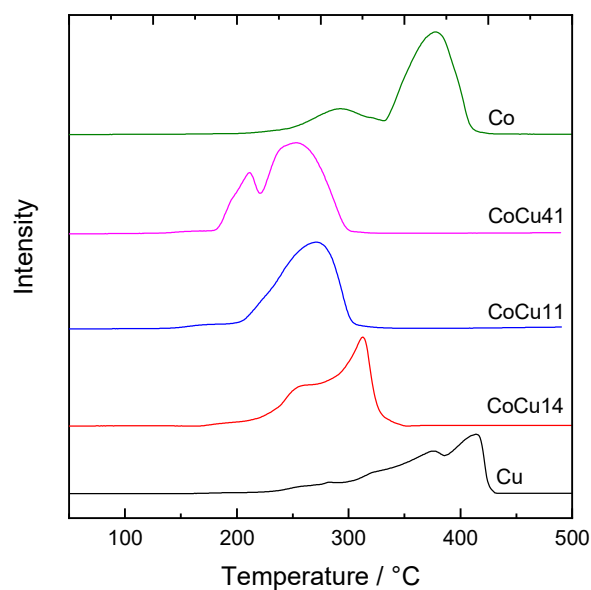


Figure 4. H₂-temperature programmed reduction profiles of the Co-Cu oxide catalysts.

Table 4. H₂-TPR parameters of the Co-Cu oxide catalysts.

Catalyst	H ₂ Consumption ^a (mmol g ⁻¹)	H ₂ Consumption ^b (mmol g ⁻¹)	Reduction Range (°C)	T _{max} ^c (°C)	T _{max} ^d (°C)
Co	16.6	16.8	170–410	378	292
CoCu41	15.8	18.1	115–300	253	214
CoCu11	14.6	16.7	130–310	271	-
CoCu14	13.4	12.5	165–350	313	260
Cu	12.6	13.8	205–450	414	375

^a theoretical; ^b experimental; ^c main reduction peak; ^d minor reduction peak.

Numerous studies have been carried out on the reducibility of bulk [4,17–21] and supported [9,10,46,47] Co-Cu mixed oxides. However, it is not easy to point out the effect of Co:Cu molar ratio on the catalyst reduction. Considering bulk Co-Cu mixed oxides, Lv et al. [9] observed easier reduction of the catalysts with increasing Co content, while Anton et al. [47] found the reverse trend, i.e., the increase in reduction temperature with increasing amount of cobalt in the catalysts. Therefore, no simple conclusion can be drawn from the effect of Co:Cu ratio on the reducibility of the mixed oxides. However, a shift in the temperature of reduction maximum was observed for the catalysts containing both Co and Cu, suggesting the interaction of both components during the reduction process. This interaction was found even during the reduction of a physical mixture of Co₃O₄ and CuO; the reduction profile of the mixture was slightly different from the superposition of reduction profiles of the single oxides [4,21]. This finding can be explained by the close contact of the oxides, which enhanced the reducibility of the single CuO and Co₃O₄. For this reason, many authors assume that the dispersion of oxides significantly affects the reduction temperature of mixtures of oxides and mixed oxides [4,9,21]. The interaction can also be demonstrated in the reduction of Co-Cu spinels [47]. In this case, the Co and Cu species are finely dispersed at atomic level, which allows a close contact between these two components and, consequently, decrease in the reduction temperature.

The decrease in the reduction temperature can be explained by a spillover effect of hydrogen in such bimetallic systems. Indeed, some metals have ability to adsorb hydrogen on their surface. This activated hydrogen spills over and promotes the reduction of another metal [23]. For the Co-Cu-O system, it is assumed that Cu²⁺ is first reduced to metallic Cu. Then, hydrogen could spill over from Cu⁰ species to cobalt oxide and

promote the reduction of Co^{3+} to Co^{2+} and/or Co^{2+} to Co^0 [22]. The spillover effect could explain the easy reduction of the CoCu41 catalyst with relatively low copper content, where the formation of highly dispersed CuO species can be expected to contribute to promote hydrogen spillover to cobalt oxide species. Indeed, the powder XRD analysis of the CoCu41 sample showed significantly higher Co:Cu molar ratio in comparison with expected nominal value of 4:1 (Table 2), which indicated formation of XRD-amorphous copper species.

Theoretical and measured hydrogen consumptions during the reduction of the Co-Cu catalysts are compared in Table 4. Theoretical hydrogen consumptions were calculated from the nominal Co:Cu molar ratios and assuming the presence of all Cu as CuO and all Co as Co_3O_4 in the catalysts. Slightly higher measured hydrogen consumptions were found in comparison with the theoretical values. Apparently, some cation-deficient oxides with excess of oxygen were formed during calcination of the coprecipitated precursors at 500 °C.

Surface composition of the catalysts was determined by XPS. The results are summarized in Table 5. The Co, Cu, Na, C, O, and N elements were detected in the XPS spectra. The Co 2p spectrum of the Co catalyst (Figure 5) corresponded to the typical spectrum of Co_3O_4 [48]. Two main peaks at 779.1 ± 0.1 and 794.1 ± 0.1 eV were attributed to Co 2p_{3/2} and Co 2p_{1/2}, respectively. The spin-orbit splitting of 15.0 eV is characteristic for the presence of both Co^{2+} and Co^{3+} cations. Low intensity of satellites indicates the presence of spinel lattice [21]. The Co-Cu catalysts showed the satellite typical for Co_3O_4 but with slightly different shape. It could be connected with Cu^{2+} cations, which may enter the surface octahedral vacancies and form Cu-O-Co species, resulting in broader and asymmetric Co 2p_{3/2} peak [49]. Fitting of the main Co 2p_{3/2} peak provided rough estimation of $\text{Co}^{2+}/\text{Co}^{3+}$ ratio (Table 5). First peak at 779.1 ± 0.1 was ascribed to Co^{3+} and the second and third peaks shifted by +1.5 eV and +3.6 eV were ascribed to Co^{2+} . The $\text{Co}^{2+}/\text{Co}^{3+}$ ratios in Table 5 indicated a slight decrease in Co^{2+} content with increased Cu content in the catalysts.

Table 5. Surface concentrations of the elements in at. % determined by XPS analysis of the examined Co-Cu oxide catalysts.

Catalyst	O	C	N	Na	Co	Cu	Co:Cu ^a	Co:Cu ^b	$\text{Co}^{2+}/\text{Co}^{3+}$
Co	51.3	21.9	1.0	5.1	20.7	0.0	-	-	0.99
CoCu41	40.5	43.8	0.0	0.0	10.9	4.8	2.3:1	4.1:1	0.98
CoCu11	32.9	53.6	0.0	1.8	6.6	5.1	1.3:1	1.0:1	0.94
CoCu14	32.2	54.3	0.4	2.5	4.1	6.5	2.6:4	1.0:4	0.88
Cu	49.2	18.2	1.6	5.5	0.0	24.8	-	-	-

^a surface molar ratio determined by XPS; ^b bulk molar ratio determined by AAS.

The XPS spectrum of the Cu catalyst showed the main peaks of Cu 2p_{3/2} at 933.5 ± 0.2 eV and Cu 2p_{1/2} at 953.3 ± 0.2 eV (Figure 6). The two satellite peaks at 941.0 and 943.5 eV with high intensity indicated the presence of CuO [48]. The XPS spectra of CoCu11 and CoCu14 samples were very similar to that of CuO but the Cu 2p_{3/2} peak was broader; the broadening could be caused by very small size of (nano)particles in the oxide of low crystallinity. The CoCu41 catalyst showed a different XPS spectrum with two additional peaks at 931 and 951 eV, indicating presence of Cu in a lower oxidation state (Cu^I or Cu^0). The measurement of Auger spectra Cu LMM showed broadening of the main peak towards 916 eV (kinetic axis) in comparison with the spectrum of Cu catalyst (Figure S1 in Supporting Information). It pointed out the presence of Cu^I (22% of total Cu). The presence of Cu_2O could be caused by the X-ray induced reduction in the presence of adventitious carbon [20]. This effect was not observed with other catalysts; the reason could be a better dispersion of CuO particles in the CoCu41 catalyst as shown by XRD. This catalyst also showed the best reducibility, which could be caused by good dispersion as well [49].

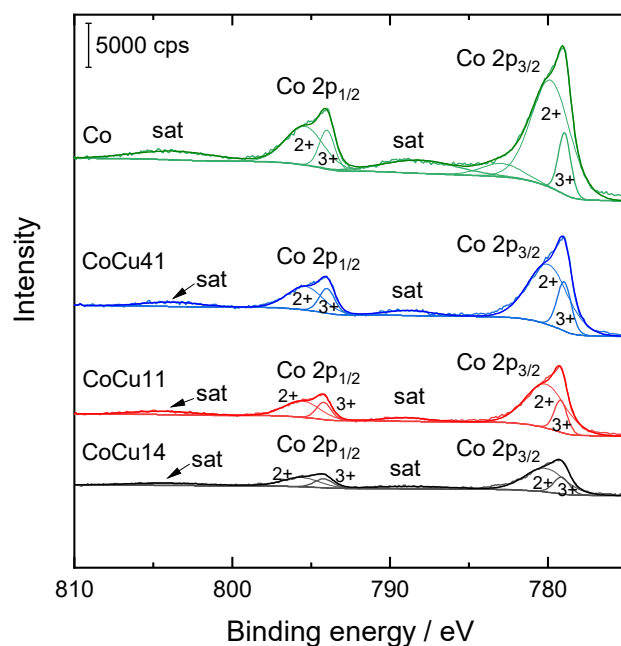


Figure 5. The Co 2p XPS spectra of the Co-Cu oxide catalysts.

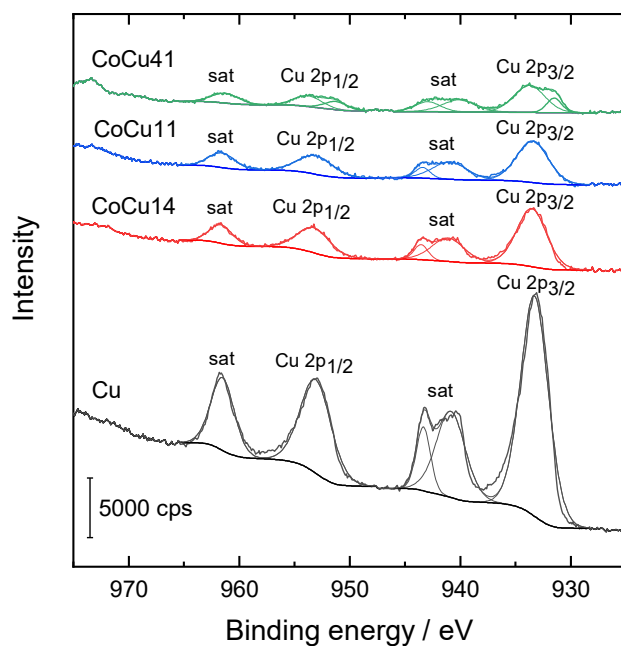


Figure 6. The Cu 2p XPS spectra of the Co-Cu oxide catalysts.

The XPS results shown in Table 5 revealed higher surface concentration of copper for the CoCu41 catalyst and higher surface concentration of cobalt for the CoCu14 catalyst compared to the bulk concentrations. A copper surface enrichment for $\text{Cu}_x\text{Co}_{3-x}\text{O}_4$ spinel has been already observed [25] for x up to 1.5. A segregation of Cu impurity on the surface of Co_3O_4 spinel after a heating treatment at 350 °C has been also reported [21]. On the other hand, to our knowledge, no segregation of cobalt on the CuO surface has been reported so far.

In all catalysts, the O 1s spectra revealed the presence of three different oxygen states. The peak at 529.4 ± 0.1 eV is characteristic for lattice oxygen, the peak at 531.0 eV is typical of surface oxygen with low coordination [50], and the peak at 532.4 eV can be attributed to oxygen in nitrates or in C–O bonds. In the Co, Cu, and CoCu14 catalysts, a peak at 407.0 eV in the N 1s region, characteristic for nitrates, was present. The Na 1s peak at 1070.8 eV

was observed in the XPS spectra of all catalysts except the CoCu41 one (Figures S2–S4 in Supporting Information). The surface concentrations of detected elements are summarized in Table 5. A strong enrichment of the surface of the CoCu41 catalyst with Cu can be seen, while the surface of the CoCu11 and especially the CoCu14 catalyst was enriched with Co.

2.2. Performance of the Catalysts in the Total Oxidation of Ethanol

The prepared Co–Cu oxide catalysts were tested in the total oxidation of ethanol. Ethanol conversion curves over the examined catalysts in dependence on reaction temperature are demonstrated in Figure 7. The activity of the catalysts was compared using the T_{50} temperature required to achieve 50% ethanol conversion and the selectivity of the catalysts using the $T_{50}(\text{CO}_2)$ and $T_{90}(\text{CO}_2)$ temperatures required to achieve 50 and 90% conversion of all organic compounds to CO_2 , respectively. Results of the catalytic measurements are summarized in Table 6. The temperature T_{50} was ranging from 91 °C (the CoCu41 catalyst) to 186 °C (the Cu catalyst). No deactivation of the catalysts was observed in the four consecutive light-off experiments. Acetaldehyde and carbon monoxide were detected as the main by-products of ethanol oxidation over the examined catalysts. Typical profiles of reactant and products concentrations during the light-off experiment over the CoCu41 catalyst are shown in Figure 8; concentration profiles measured over the other catalysts are presented in Supporting Information (Figures S5–S8). The most active CoCu41 catalyst exhibited the highest maximum acetaldehyde formation among the Co–Cu oxides (444 ppm), while the single-component Co and Cu catalysts showed even higher acetaldehyde concentrations (544 and 541 ppm, respectively). The amounts of carbon monoxide formed during the ethanol oxidation over the examined catalysts were low (the maximum concentrations were ranging between 5 ppm and 14 ppm, except the Co catalyst exhibiting 131 ppm of CO).

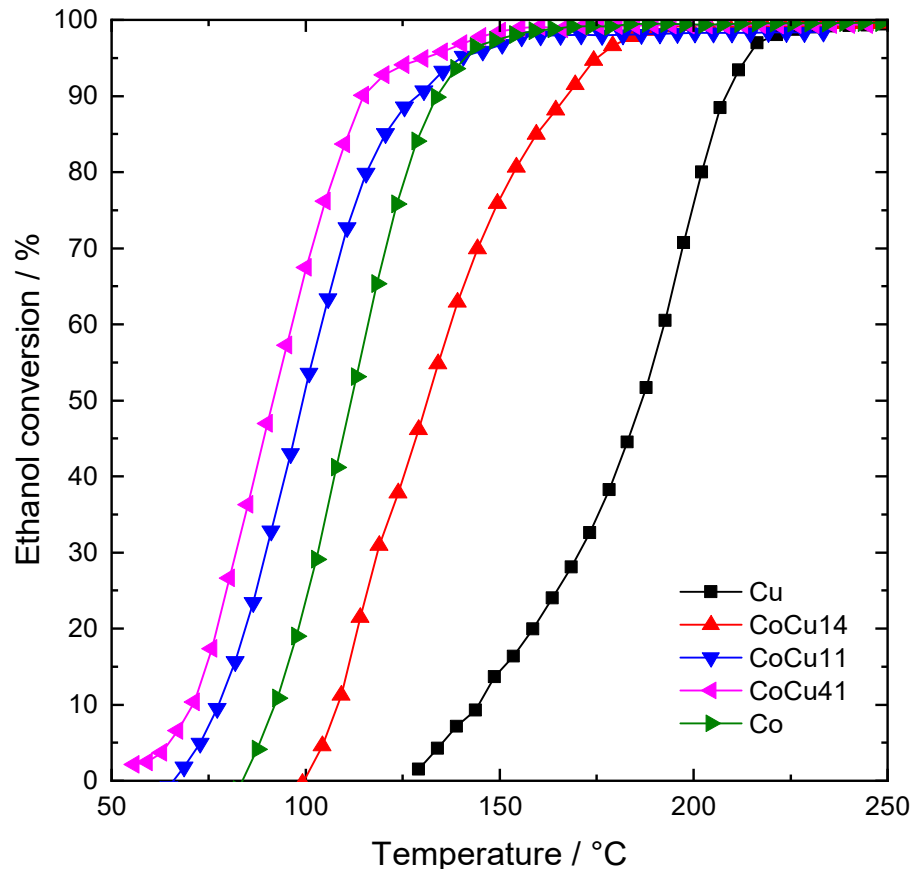
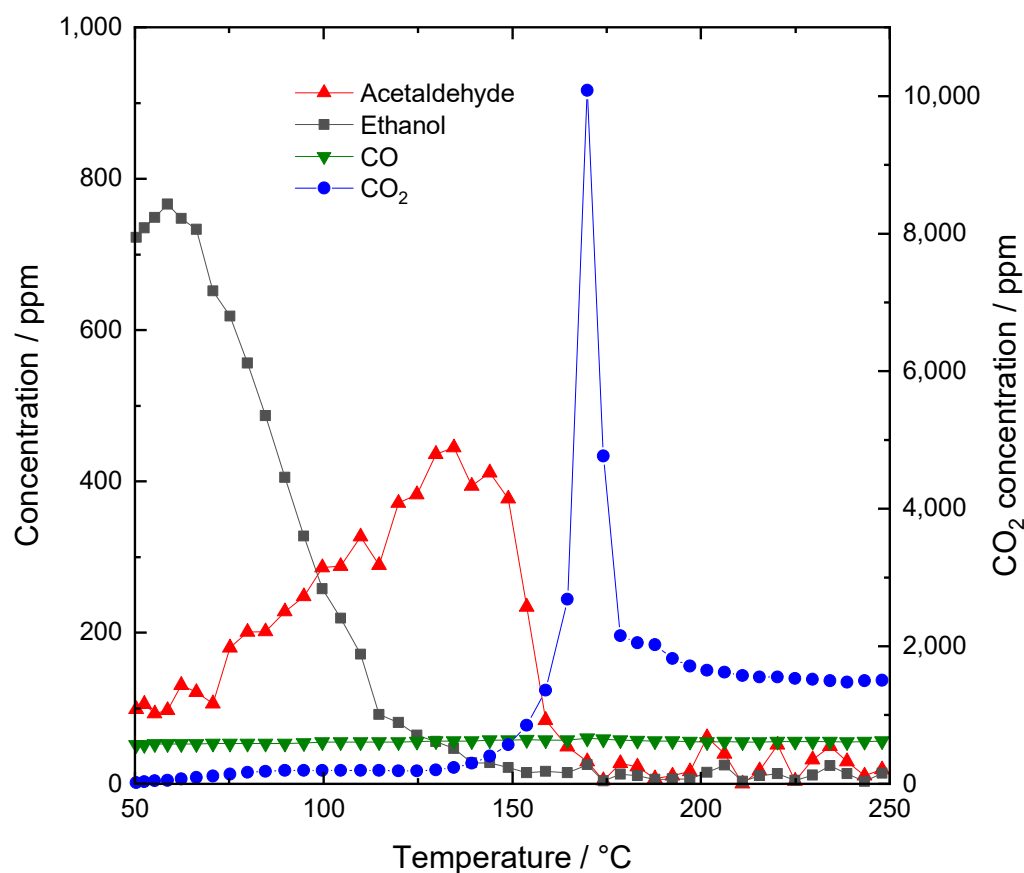


Figure 7. Light-off curves of ethanol oxidation over the examined catalysts.

Table 6. Catalytic properties of the examined Co-Cu oxide catalysts (oxidation of 750 ppm of ethanol in air at GHSV of $20 \text{ l}_{\text{gcat}}^{-1} \text{ h}^{-1}$).

Catalyst	T_{50} (°C)	$T_{50}(\text{CO}_2)$ (°C)	$T_{90}(\text{CO}_2)$ (°C)	$\text{AcA}_{\text{max}}^{\text{a}}$ (ppm)	$T_{\text{max}}^{\text{b}}$ (°C)	$\text{CO}_{\text{max}}^{\text{c}}$ (ppm)	$T_{\text{max}}^{\text{d}}$ (°C)
Co	111	187	202	544	137	131	202
CoCu41	91	152	159	444	134	7	170
CoCu11	99	165	172	428	141	7	171
CoCu14	131	189	197	340	164	12	199
Cu	186	228	259	541	212	9	216

^a maximum concentration of acetaldehyde during the experiment; ^b temperature, at which the maximum concentration of acetaldehyde was achieved; ^c maximum concentration of carbon monoxide during the experiment; ^d temperature, at which the maximum concentration of CO was achieved.

**Figure 8.** Concentration profiles of ethanol, acetaldehyde, carbon monoxide, and carbon dioxide during the light-off experiment over the CoCu41 catalyst.

The selectivity of the catalysts was evaluated using the temperature needed to achieve 50% conversion to carbon dioxide. The $T_{50}(\text{CO}_2)$ was increasing in the order $\text{CoCu41} < \text{CoCu11} < \text{Co} \approx \text{CoCu14} < \text{Cu}$. Nevertheless, the purpose of VOC abatement is the complete oxidation of ethanol to carbon dioxide and water. Therefore, the $T_{90}(\text{CO}_2)$ temperature, at which 90% conversion of all organic compounds to CO_2 was achieved, represents an important parameter that indicates the performance of the catalysts in the total oxidation. The lowest $T_{90}(\text{CO}_2)$ temperature (159°C) was observed for the cobalt-rich CoCu41 catalyst, while 197 and 259°C were found for the CoCu14 and Cu catalysts, respectively. Although the Co catalyst was quite active (T_{50} temperature 111°C), a rather high $T_{90}(\text{CO}_2)$ temperature (202°C) was found for this catalyst. Compared to the single-component Co catalyst, the best Co-Cu oxide catalyst (CoCu41 sample) exhibited a better catalytic performance (the T_{50} temperature was 20°C lower and the $T_{90}(\text{CO}_2)$ temperature was 43°C lower). An even greater difference was found between the single-component Cu

catalyst and the CoCu41 catalyst; the Cu catalyst showed T_{50} and $T_{90}(CO_2)$ temperatures of about 100 °C higher compared to the CoCu41 sample. This is an important parameter with regard to the potential industrial applications as a lower operation temperature reduces energy costs. The findings further confirmed the synergistic effect of Co_3O_4 and CuO in some mixed oxide catalysts. The cobalt oxide-based catalyst was highly active but with low selectivity, while the copper oxide-based catalyst showed rather weak activity but good selectivity. The Co-Cu oxide catalysts with Co:Cu molar ratio of 4:1 and 1:1 allowed high activity and good selectivity to be achieved at the same time. Their T_{50} temperatures for ethanol oxidation were much lower than those of CuO and lower than those of Co_3O_4 , while their selectivity in terms of $T_{50}(CO_2)$ and $T_{90}(CO_2)$ temperatures was much better compared to the single-component Cu and Co catalysts.

3. Discussion

The Co-Cu oxide catalysts with various Co:Cu molar ratios were prepared by calcination of coprecipitated precursors and compared with the single-component Co and Cu oxides. A possible synergistic effect between copper and cobalt components was studied, as such synergistic effect was already reported by Jia et al. [8] for toluene and ethyl acetate oxidation. They suggested that the fine dispersion of CuO particles on the surface of the Co_3O_4 , which might lead to formation of Cu-Co spinel, probably caused an increase in the surface area and improved catalytic activity. However, our measured powder XRD patterns and Raman spectra of the examined Co-Cu oxide catalysts indicated that mixtures of Co_3O_4 and CuO rather than Co-Cu mixed oxides were formed after the coprecipitated precursors calcination at 500 °C (Figures 1 and 2). Furthermore, the largest BET surface area exhibited the single-component Co sample (Table 3), while the best catalytic performance was achieved with the CoCu41 catalyst (Table 6). On the contrary, a shift in the temperature of reduction maximum in the H_2 -TPR profiles of the Co-Cu catalysts indicated an interaction between Co_3O_4 and CuO components during the reduction process (Figure 4). The easy reduction of the CoCu41 catalyst was tentatively ascribed to the formation of highly dispersed CuO species that promote hydrogen spillover from Cu to cobalt oxide species. Moreover, the evaluation of powder XRD data showed a lower amount of CuO in the CoCu41 catalyst compared to the bulk Co:Cu molar ratio determined by AAS (Table 2). Finally, the CoCu41 catalyst was the only one to show the XPS spectrum with two additional peaks at 931 eV and 951 eV (Figure 6), indicating the presence of Cu in a lower oxidation state (Cu^I or Cu^0). Again, this difference can be explained by the better dispersion of CuO particles in the CoCu41 catalyst. Besides the work of Jia et al. [8], the synergistic effect of highly dispersed CuO_x phase in the Co-Cu catalyst was recently observed by More et al. [46] for the low temperature oxidation of CO, propene, and toluene. The Co-Cu catalyst with highly dispersed CuO_x phase showed more labile surface oxygen, which was advantageous for the oxidation reaction. Thus, the high activity and selectivity of the CoCu41 catalyst could be ascribed to the presence of finely dispersed CuO particles on the surface of Co_3O_4 .

The dependence of the $T_{50}(CO_2)$ temperature on the temperature of the reduction onset in the H_2 -TPR experiments (cf. the reduction range in Table 4) is shown in Figure 9. Formerly we observed a good correlation between the position of the first reduction peak in H_2 -TPR experiments and the T_{50} temperature during ethanol oxidation [51], which pointed to the Mars–van Krevelen reaction mechanism. Thus, considering the linear correlation shown in Figure 9, the redox mechanism can be expected also for ethanol oxidation over the Co-Cu oxide catalysts.

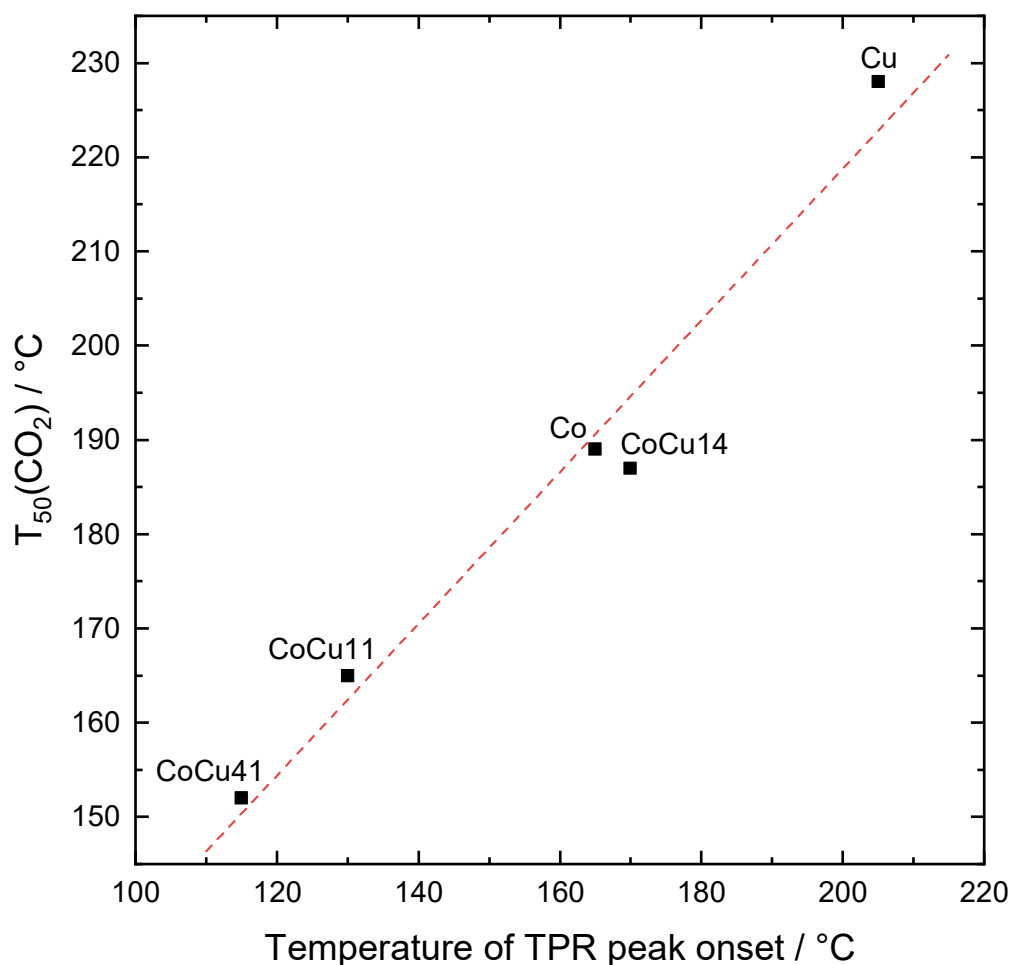


Figure 9. Correlation between the temperature of the reduction onset in the H₂-TPR experiments and the T₅₀(CO₂) temperature, at which 50% conversion of ethanol to CO₂ was achieved.

4. Materials and Methods

4.1. Catalysts Preparation

The precursors were prepared by coprecipitation of aqueous cobalt and copper nitrate solutions; appropriate amounts of Co(NO₃)₂·6H₂O and Cu(NO₃)₂·3H₂O were dissolved in distilled water to obtain solutions with desired Co:Cu molar ratios and total concentration of metal cations 1.0 mol L⁻¹. The solution (450 mL) was added with the flow rate of 7.5 mL min⁻¹ to the stirred batch reactor containing 200 mL of distilled water. The reaction pH of 10.0 ± 0.1 was maintained by simultaneous addition of aqueous solution containing NaOH (3.0 mol L⁻¹) and Na₂CO₃ (0.5 mol L⁻¹). The reaction was carried out under vigorous stirring at room temperature. The resulting suspension was stirred for 1 h at room temperature; the product was then filtered off, thoroughly washed with distilled water, and dried overnight at 60 °C. The dried products were calcined at 500 °C for 4 h in air. After cooling, the calcined pellets were crushed and sieved to obtain fraction with particle size of 0.160–0.315 mm, which was used in catalytic measurements. The Co–Cu oxide catalysts with Co:Cu molar ratios of 4:1, 1:1, and 1:4 were labeled as CoCu41, CoCu11, and CoCu14, respectively. Single-component cobalt and copper oxide catalysts were prepared in the same way and labeled as Co and Cu, respectively. The samples of coprecipitated precursors (before calcination) were denoted with the suffix “P” (e.g., CoCu41-P).

4.2. Catalyst Characterization

Content of metal cations (Co, Cu, and Na) in the prepared samples was determined by atomic absorption spectroscopy (AAS). The washed and dried precursors (about 0.01 g)

were powdered and dissolved in 2 mL of 65% HNO₃ and warmed up in the water bath; H₂O₂ (1 mL) was added to complete the sample dissolution. Then the beaker content was quantitatively poured into 50 mL flask and filled up with distilled water. Concentration of metal cations was measured using Agilent 280 FS AA spectrometer with flame atomization technique. The content of metal cations in oxide catalysts was calculated using the weight loss determined after 4 h calcination of the precursors at 500 °C in air.

Powder X-ray diffraction (XRD) patterns were measured by AXS D8 (Bruker) diffractometer (Bruker, Berlin, Germany) using Co K α radiation ($\lambda = 0.179$ nm) in the range from 10 to 80° 2 θ (step size 0.02°). The qualitative analysis was performed using HighScore Plus 4.8 software package (PANalytical). The lattice parameters were obtained from cell refinement of attributed phase after default line profile fitting in HighScore Plus software (PANalytical, Malvern, Almelo, The Netherlands, 2018). The full width in half maximum (FWHM) values and crystallite sizes were evaluated using the same software. The crystallite sizes of Co₃O₄-like oxides were calculated as a mean coherence length in [311] direction (the most intense diffraction line of cubic spinel); the crystallite sizes of CuO (tenorite) were calculated as a mean coherence length in [−202] direction.

Surface composition of Co-Cu oxides was analyzed using the X-ray photoelectron spectroscopy (XPS). The measurements were carried out using AXIS Ultra DLD Kratos spectrometer equipped with a monochromatic Al K α source ($h\nu = 1486.6$ eV) operating at 180 W. The XPS spectra were recorded at ambient temperature, while using an ultra-high vacuum system (base pressure 10^{−9} mbar). The Co, Cu, O, N, Na, and C elements were detected. The calibration for charging effect was carried out based on binding energy of adventitious carbon C 1s peak located at 284.8 eV. The XPS data evaluation was performed using CasaXPS software.

Surface area and textural properties of the catalysts were determined from nitrogen adsorption-desorption isotherms at 77 K using Micromeritics Tristar II Surface Areas and Porosity apparatus (Norcross, Atlanta, GA, Micromeritics, USA). Surface area S_{BET} was calculated by the BET method. Pore size and volume distribution were calculated using the BJH method. The samples (about 0.20 g) were outgassed in vacuum at 150 °C prior to data collection.

Temperature-programmed reduction (H₂-TPR) measurements were carried out using AutoChem II 2920 V3.05 equipment (Micromeritics) with a H₂/Ar mixture (5 mol. % H₂), flow rate 50 mL min^{−1} and linear temperature increase 10 °C min^{−1} in temperature range from 25 to 700 °C. The amount of analyzed sample was approximately 15 mg.

Raman spectra were recorded on Horiba Xplora spectrometer. The 785 nm laser was used for excitation, the power on the sample was adjusted by 1% filter. The laser beam was focused on the surface of the sample using 100 × microscope objective (NA 0.9). Due to various stability of the samples, the acquisition times were used as follows: 30 s for Co, 600 s for Cu, and 1800 s for CoCu41, CoCu11, and CoCu14 oxide samples. The Raman signal was collected in backscattering mode using the same objective through a confocal hole of 200 μ m diameter. The scattered light was dispersed via a spectrometer equipped with 1200 grooves grating.

4.3. Catalytic Experiments

The catalysts (0.2 g) in the form of 0.160–0.315 mm grains were tested in a fixed bed reactor (5 mm inner diameter) over a temperature range of 50–400 °C with a temperature ramp of 2 °C min^{−1} at a space velocity (GHSV) of 20 L g^{−1} h^{−1} and an inlet ethanol concentration in air of 750 ppm (details are described elsewhere [52]). All experiments were started at 50 °C after the equilibrium adsorption of ethanol at this temperature was reached. The composition of the reaction mixture was analyzed by the Agilent 8890 gas chromatograph (Agilent Technologies, Santa Clara, CA, USA) coupled with a mass spectrometer. The T_{50} temperature, at which 50% ethanol conversion was achieved, was used to compare the catalytic performance of the catalysts. The $T_{50}(\text{CO}_2)$ and $T_{90}(\text{CO}_2)$ temperatures, at which

50 and 90% conversion of ethanol to CO₂ was achieved, were employed to compare the selectivity of the catalysts.

5. Conclusions

The Co-Cu oxide catalysts with various Co:Cu molar ratios were prepared by calcination of coprecipitated precursors and compared with the single-component Co and Cu oxides. Both powder XRD patterns and Raman spectra indicated that the Co-Cu catalysts contained a mixture of Co₃O₄ and CuO. The surface area of the single-component oxides showed a marked difference (27 and 5 m² g⁻¹ was found for the Co and Cu catalysts, respectively), while the surface area of all Co-Cu catalysts was very similar (18–21 m² g⁻¹). Temperature-programmed reduction by hydrogen proved that CuO promoted the reduction of Co₃O₄ in the Co-Cu oxides. The CoCu41 catalyst with a Co:Cu molar ratio of 4:1 was reduced at the lowest temperature, likely due to a high dispersion of CuO. The CuO content evaluated from powder XRD data was significantly lower in comparison with bulk Co:Cu molar ratio determined by AAS; it indicated the formation of XRD-amorphous copper species. The XPS results confirmed the presence of the electronic surface states of Co and Cu similar to those in Co₃O₄ and CuO in all Co-Cu oxide catalysts. Moreover, a strong Cu enrichment was observed on the surface of the CoCu41 catalyst. Finally, unlike all other catalysts, the XPS spectra of the CoCu41 catalyst showed the presence of Cu in a lower oxidation state (Cu^I or Cu⁰), likely due to high dispersion of CuO.

The single-component Co and Cu catalysts showed 50% ethanol conversion at 111 and 186 °C, respectively, whereas the *T*₅₀ temperatures between 91 and 131 °C were found for the Co-Cu oxide catalysts. A synergistic effect of the two components was observed for catalysts with Co:Cu molar ratio of 4:1 and 1:1. Although the Co oxide catalyst was quite active (*T*₅₀ of 111 °C), the temperature required to achieve 90% conversion to CO₂ was high (202 °C). Remarkably, with the CoCu41 catalyst, the *T*₉₀(CO₂) was achieved already at 159 °C. This is an important result with regard to potential industrial applications: a lower operation temperature reduces energy costs of the catalytic abatement technology. Furthermore, these findings confirm the synergistic effect of Co₃O₄ and CuO in some of the catalysts (the *T*₉₀(CO₂) for the Cu oxide catalyst was 259 °C). Although the formation of the mixed Co-Cu oxides was not revealed, the high activity and selectivity of the CoCu41 catalyst was ascribed to the presence of finely dispersed CuO particles on the surface of the Co₃O₄ as indicated by XRD, H₂-TPR, and XPS.

Supplementary Materials: The following supporting information can be downloaded at: <https://www.mdpi.com/article/10.3390/catal13010107/s1>, Figure S1: The Cu LMM XPS spectra of the Co-Cu oxide catalysts; Figure S2: The Na 1 s XPS spectra of the Co-Cu oxide catalysts; Figure S3: The N 1 s XPS spectra of the Co-Cu oxide catalysts; Figure S4: The O 1 s XPS spectra of the Co-Cu oxide catalysts; Figure S5: Concentration profiles of ethanol, acetaldehyde, carbon monoxide, and carbon dioxide during the light-off experiment over the Co catalyst; Figure S6: Concentration profiles of ethanol, acetaldehyde, carbon monoxide, and carbon dioxide during the light-off experiment over the CoCu11 catalyst; Figure S7: Concentration profiles of ethanol, acetaldehyde, carbon monoxide, and carbon dioxide during the light-off experiment over the CoCu14 catalyst; Figure S8: Concentration profiles of ethanol, acetaldehyde, carbon monoxide, and carbon dioxide during the light-off experiment over the Cu catalyst.

Author Contributions: Conceptualization, F.K.; methodology, F.K., M.K., K.J. and J.-F.L.; validation, F.K., J.M., J.-M.G. and K.J.; investigation, K.K., J.B., J.M. and M.K.; data curation, K.K., J.-M.G. and M.K.; writing—original draft preparation, K.K. and P.T.; writing—review and editing, K.J., J.-F.L. and F.K.; supervision, F.K. and J.-F.L.; project administration, F.K. and J.-F.L. All authors have read and agreed to the published version of the manuscript.

Funding: This research was funded by Czech Science Foundation (project 21-04477S) and the PHC Barrande 2022 between the University of Chemistry and Technology, Prague and University of Lille (project 8J22FR005/48096PE, Ministry of Education, Youth and Sports of the Czech Republic, Ministry of Europe and Foreign Affairs (MEAE) and the Ministry of Higher Education, Research and Innovation (MESRI) of France.

Data Availability Statement: The data will be made available on request.

Acknowledgments: The authors thank Hana Šnajdaufová for the characterization of porous structure of catalysts and Ladislav Lapčák for the measurement of Raman spectra.

Conflicts of Interest: The authors declare that they have no known competing financial interests or personal relationships that could have appeared to influence the work reported in this article. The funders had no role in the design of the study; in the collection, analyses, or interpretation of data; in the writing of the manuscript; or in the decision to publish the results.

References

1. Kamal, M.S.; Razzak, S.A.; Hossain, M.M. Catalytic oxidation of volatile organic compounds (VOCs)—A review. *Atmos. Environ.* **2016**, *140*, 117. [[CrossRef](#)]
2. Liotta, L.F. Catalytic oxidation of volatile organic compounds on supported noble metals. *Appl. Catal. B* **2010**, *100*, 403–412. [[CrossRef](#)]
3. Gaálová, J.; Topka, P. Gold and Ceria as Catalysts for VOC Abatement: A Review. *Catalysts* **2021**, *11*, 789. [[CrossRef](#)]
4. Hosseini, S.A.; Niaei, A.; Salari, D.; Alvarez-Galvan, M.C.; Fierro, J.L.G. Study of correlation between activity and structural properties of Cu-(Cr, Mn and Co)₂ nano mixed oxides in VOC combustion. *Ceram. Int.* **2014**, *40*, 6157–6163. [[CrossRef](#)]
5. Zavyalova, U.; Nigrovski, B.; Pollok, K.; Langenhorst, F.; Müller, B.; Scholz, P.; Ondruschka, B. Gel-combustion synthesis of nanocrystalline spinel catalysts for VOCs elimination. *Appl. Catal. B* **2008**, *83*, 221–228. [[CrossRef](#)]
6. Varghese, S.; Cutrufello, M.G.; Rombi, E.; Cannas, C.; Monaci, R.; Ferino, I. CO oxidation and preferential oxidation of CO in the presence of hydrogen over SBA-15-templated CuO-Co₃O₄ catalysts. *Appl. Catal. A* **2012**, *443–444*, 161–170. [[CrossRef](#)]
7. Lu, C.-Y.; Tseng, H.-H.; Wey, M.-Y.; Liu, L.-Y.; Kuo, J.-H.; Chuang, K.-H. Al₂O₃-supported Cu–Co bimetallic catalysts prepared with polyol process for removal of BTEX and PAH in the incineration flue gas. *Fuel* **2009**, *88*, 340–347. [[CrossRef](#)]
8. Jia, L.; Guo, Y.; Tran, T.P.; Sakurai, M.; Kameyama, H. Synergistic Effect of Copper and Cobalt in Cu-Co Bulk Oxide Catalyst for Catalytic Oxidation of Volatile Organic Compounds. *J. Chem. Eng. Jpn.* **2012**, *45*, 590–596. [[CrossRef](#)]
9. Lv, Y.; Liu, L.; Zhang, H.; Yao, X.; Gao, F.; Yao, K.; Dong, L.; Chen, Y. Investigation of surface synergetic oxygen vacancy in CuO–CoO binary metal oxides supported on γ -Al₂O₃ for NO removal by CO. *J. Colloid Interface Sci.* **2013**, *390*, 158–169. [[CrossRef](#)]
10. Carrillo, A.M.; Carriazo, J.G. Cu and Co oxides supported on halloysite for the total oxidation of toluene. *Appl. Catal. B* **2015**, *164*, 443–452. [[CrossRef](#)]
11. Li, S.; Wang, H.; Li, W.; Wu, X.; Tang, W.; Chen, Y. Effect of Cu substitution on promoted benzene oxidation over porous CuCo-based catalysts derived from layered double hydroxide with resistance of water vapour. *Appl. Catal. B* **2015**, *166–167*, 260–269. [[CrossRef](#)]
12. Topka, P.; Dvořáková, M.; Kšírová, P.; Perekrestov, R.; Čada, M.; Balabánová, J.; Koštejn, M.; Jiráťová, K.; Kovanda, F. Structured cobalt oxide catalysts for VOC abatement: The effect of preparation method. *Environ. Sci. Pollut. Res.* **2020**, *27*, 7608–7617. [[CrossRef](#)]
13. Dvořáková, M.; Perekrestov, R.; Kšírová, P.; Balabánová, J.; Jiráťová, K.; Maixner, J.; Topka, P.; Rathouský, J.; Koštejn, M.; Čada, M.; et al. Preparation of cobalt oxide catalysts on stainless steel wire mesh by combination of magnetron sputtering and electrochemical deposition. *Catal. Today* **2019**, *334*, 13–23. [[CrossRef](#)]
14. Kovanda, F.; Jiráťová, K.; Ludvíková, J.; Raabová, H. Co-Mn-Al mixed oxides on anodized aluminum supports and their use as catalysts in the total oxidation of ethanol. *Appl. Catal. A* **2013**, *464*, 181–190. [[CrossRef](#)]
15. Jiráťová, K.; Perekrestov, R.; Dvořáková, M.; Balabánová, J.; Koštejn, M.; Veselý, M.; Čada, M.; Topka, P.; Pokorná, D.; Hubička, Z.; et al. Modification of Cobalt Oxide Electrochemically Deposited on Stainless Steel Meshes with Co-Mn Thin Films Prepared by Magnetron Sputtering: Effect of Preparation Method and Application to Ethanol Oxidation. *Catalysts* **2021**, *11*, 1453. [[CrossRef](#)]
16. Topka, P.; Jiráťová, K.; Dvořáková, M.; Balabánová, J.; Koštejn, M.; Kovanda, F. Hydrothermal deposition as a novel method for the preparation of Co-Mn mixed oxide catalysts supported on stainless steel meshes: Application to VOC oxidation. *Environ. Sci. Pollut. Res.* **2022**, *29*, 5172–5183. [[CrossRef](#)]
17. Li, D.; Liu, X.; Zhang, Q.; Wang, Y.; Wan, H. Cobalt and Copper Composite Oxides as Efficient Catalysts for Preferential Oxidation of CO in H₂-Rich Stream. *Catal. Lett.* **2009**, *127*, 377–385. [[CrossRef](#)]
18. Wang, Y.; Liu, X.; Hu, X.; Wu, R.; Zhao, Y. Preparation and characterization of Cu–Mn composite oxides in N₂O decomposition. *React. Kinet. Mech. Cat.* **2020**, *129*, 165–179. [[CrossRef](#)]
19. Chen, C.; Liu, L.; Li, Y.; Li, W.; Zhou, L.; Lan, Y.; Li, Y. Insight into heterogeneous catalytic degradation of sulfamethazine by peroxymonosulfate activated with CuCo₂O₄ derived from bimetallic oxalate. *Chem. Eng. J.* **2020**, *384*, 123257. [[CrossRef](#)]
20. Rosa-Toro, A.; Berenguer, R.; Quijada, C.; Montilla, F.; Morallón, E.; Vázquez, J.L. Preparation and Characterization of Copper-Doped Cobalt Oxide Electrodes. *J. Phys. Chem. B* **2006**, *110*, 24021–24029. [[CrossRef](#)]
21. Yuan, R.-M.; Li, H.-J.; Yin, X.-M.; Wang, H.-Q.; Lu, J.-H.; Zhang, L. Coral-like Cu-Co-mixed oxide for stable electro-properties of glucose determination. *Electrochim. Acta* **2018**, *273*, 502–510. [[CrossRef](#)]
22. Paknahad, P.; Askari, M.; Ghorbanzadeh, M. Characterization of nanocrystalline CuCo₂O₄ spinel prepared by sol-gel technique applicable to the SOFC interconnect coating. *Appl. Phys. A Mater. Sci. Process.* **2015**, *119*, 727–734. [[CrossRef](#)]

23. Berenguer, R.; Quijada, C.; La Rosa-Toro, A.; Morallón, E. Electro-oxidation of cyanide on active and non-active anodes: Designing the electrocatalytic response of cobalt spinels. *Sep. Purif. Technol.* **2019**, *208*, 42–50. [[CrossRef](#)]
24. Deng, X.; Dodekatos, G.; Pupovac, K.; Weidenthaler, C.; Schmidt, W.N.; Schüth, F.; Tüysüz, H. Pseudomorphic Generation of Supported Catalysts for Glycerol Oxidation. *ChemCatChem* **2015**, *7*, 3832–3837. [[CrossRef](#)]
25. Wang, J.; Chernavskii, P.A.; Khodakov, A.Y.; Wang, Y. Structure and catalytic performance of alumina-supported copper–cobalt catalysts for carbon monoxide hydrogenation. *J. Catal.* **2012**, *286*, 51–61. [[CrossRef](#)]
26. Alvarez, A.; Ivanova, S.; Centeno, M.A.; Odriozola, J.A. Sub-ambient CO oxidation over mesoporous Co₃O₄: Effect of morphology on its reduction behavior and catalytic performance. *Appl. Catal. A* **2012**, *431–432*, 9–17. [[CrossRef](#)]
27. Wang, G.; Shen, X.; Horvat, J.; Wang, B.; Liu, H.; Wexler, D.; Yao, J. Hydrothermal Synthesis and Optical, Magnetic, and Supercapacitance Properties of Nanoporous Cobalt Oxide Nanorods. *J. Phys. Chem. C* **2009**, *113*, 4357–4361. [[CrossRef](#)]
28. Torres-Luna, J.A.; Giraldo-Gómez, G.I.; Sanabria-González, N.R.; Carriazo, J.G. Catalytic degradation of real-textile azo-dyes in aqueous solutions by using Cu–Co/halloysite. *Bull. Mater. Sci.* **2019**, *42*, 137. [[CrossRef](#)]
29. Rashad, M.; Rüsing, M.; Berth, G.; Lischka, K.; Pawlis, A. CuO and Co₃O₄ Nanoparticles: Synthesis, Characterizations, and Raman Spectroscopy. *J. Nanomater.* **2013**, *2013*, 714853. [[CrossRef](#)]
30. Xu, J.F.; Ji, W.; Shen, Z.X.; Li, W.S.; Tang, S.H.; Ye, X.R.; Jia, D.Z.; Xin, X.Q. Raman spectra of CuO nanocrystals. *J. Raman Spectrosc.* **1999**, *30*, 413–415. [[CrossRef](#)]
31. Silambarasan, M.; Padmanathan, N.; Ramesh, P.S.; Geetha, D. Spinel CuCo₂O₄ Nanoparticles: Facile One-Step Synthesis, Optical, and Electrochemical properties. *Mater. Res. Express* **2016**, *3*, 095021. [[CrossRef](#)]
32. Su, J.; Zhang, Z.; Fu, D.; Liu, D.; Xu, X.-C.; Shi, B.; Wang, X.; Si, R.; Jiang, Z.; Xu, J.; et al. Higher alcohols synthesis from syngas over CoCu/SiO₂ catalysts: Dynamic structure and the role of Cu. *J. Catal.* **2016**, *336*, 94–106. [[CrossRef](#)]
33. Thommes, M.; Kaneko, K.; Neimark, A.V.; Olivier, J.P.; Rodriguez-Reinoso, F.; Rouquerol, J.; Sing, K.S.W. Physisorption of gases, with special reference to the evaluation of surface area and pore size distribution (IUPAC Technical Report). *Pure Appl. Chem.* **2015**, *87*, 1051–1069. [[CrossRef](#)]
34. Sahooli, M.; Sabbaghi, S.; Saboori, R. Synthesis and characterization of mono sized CuO nanoparticles. *Mater. Lett.* **2012**, *81*, 169–172. [[CrossRef](#)]
35. Molavi, R.; Sheikhi, M.H. Facile wet chemical synthesis of Al doped CuO nanoleaves for carbon monoxide gas sensor applications. *Mater. Sci. Semicond. Process.* **2020**, *106*, 104767. [[CrossRef](#)]
36. Kim, M.H.; Cho, K.H.; Shin, C.-H.; Kang, S.-E.; Ham, S.-W. Total oxidation of propane over Cu-Mn mixed oxide catalysts prepared by co-precipitation method. *Korean J. Chem. Eng.* **2011**, *28*, 1139–1143. [[CrossRef](#)]
37. Meshram, S.P.; Adhyapak, P.V.; Mulik, U.P.; Amalnerkar, D.P. Facile synthesis of CuO nanomorphs and their morphology dependent sunlight driven photocatalytic properties. *Chem. Eng. J.* **2012**, *204–206*, 158–168. [[CrossRef](#)]
38. Liotta, L.F.; Di Carlo, G.; Pantaleo, G.; Venezia, A.M.; Deganello, G. Co₃O₄/CeO₂ composite oxides for methane emissions abatement: Relationship between Co₃O₄–CeO₂ interaction and catalytic activity. *Appl. Catal. B Environ.* **2006**, *66*, 217–227. [[CrossRef](#)]
39. de Rivas, B.; López-Fonseca, R.; Jiménez-González, C.; Gutiérrez-Ortiz, J.I. Synthesis, characterisation and catalytic performance of nanocrystalline Co₃O₄ for gas-phase chlorinated VOC abatement. *J. Catal.* **2011**, *281*, 88–97. [[CrossRef](#)]
40. Zheng, Y.; Yu, Y.; Zhou, H.; Huang, W.; Pu, Z. Combustion of lean methane over Co₃O₄ catalysts prepared with different cobalt precursors. *RSC Adv.* **2020**, *10*, 4490–4498. [[CrossRef](#)]
41. Pu, Z.; Zhou, H.; Zheng, Y.; Huang, W.; Li, X. Enhanced methane combustion over Co₃O₄ catalysts prepared by a facile precipitation method: Effect of aging time. *Appl. Surf. Sci.* **2017**, *410*, 14–21. [[CrossRef](#)]
42. Ordóñez, S.; Paredes, J.R.; Díez, F.V. Sulphur poisoning of transition metal oxides used as catalysts for methane combustion. *Appl. Catal. A Gen.* **2008**, *341*, 174–180. [[CrossRef](#)]
43. Stelmachowski, P.; Ciura, K.; Grzybek, G. Morphology-dependent reactivity of cobalt oxide nanoparticles in N₂O decomposition. *Catal. Sc. Technol.* **2016**, *6*, 5554–5560. [[CrossRef](#)]
44. Megía, P.J.; Carrero, A.; Calles, J.A.; Vizcaíno, A.J. Hydrogen Production from Steam Reforming of Acetic Acid as a Model Compound of the Aqueous Fraction of Microalgae HTL Using Co-M/SBA-15 (M: Cu, Ag, Ce, Cr) Catalysts. *Catalysts* **2019**, *9*, 1013. [[CrossRef](#)]
45. Fei, Z.; Liu, H.; Dai, Y.; Ji, W.; Chen, X.; Tang, J.; Cui, M.; Qiao, X. Efficient catalytic oxidation of HCl to recycle Cl₂ over the CuO–CeO₂ composite oxide supported on Y type zeolite. *Chem. Eng. J.* **2014**, *257*, 273–280. [[CrossRef](#)]
46. More, R.K.; Lavande, N.R.; More, P.M. Copper supported on Co substituted hydroxyapatite for complete oxidation of diesel engine exhaust and VOC. *Mol. Catal.* **2019**, *474*, 110414. [[CrossRef](#)]
47. Anton, J.; Nebel, J.; Song, H.; Froese, C.; Weide, P.; Ruland, H.; Muhler, M.; Kaluza, S. Structure–activity relationships of Co-modified Cu/ZnO/Al₂O₃ catalysts applied in the synthesis of higher alcohols from synthesis gas. *Appl. Catal. A* **2015**, *505*, 326–333. [[CrossRef](#)]
48. Biesinger, M.C.; Lau, L.W.M.; Gerson, A.R.; Smart, R.S.C. Resolving surface chemical states in XPS analysis of first row transition metals, oxides and hydroxides: Sc, Ti, V, Cu and Zn. *Appl. Surf. Sci.* **2010**, *257*, 887–898. [[CrossRef](#)]
49. Amri, A.; Duan, X.; Yin, C.-Y.; Jiang, Z.-T.; Rahman, M.M.; Pryor, T. Solar absorptance of copper–cobalt oxide thin film coatings with nano-size, grain-like morphology: Optimization and synchrotron radiation XPS studies. *Appl. Surf. Sci.* **2013**, *275*, 127–135. [[CrossRef](#)]

50. Petitto, S.C.; Langell, M.A. Surface composition and structure of $\text{Co}_3\text{O}_4(110)$ and the effect of impurity segregation. *J. Vacuum Sci. Technol. A* **2004**, *22*, 1690–1696. [[CrossRef](#)]
51. Gaálová, J.; Topka, P.; Kaluža, L.; Soukup, K.; Barbier, J. Effect of gold loading on ceria-zirconia support in total oxidation of VOCs. *Catal. Today* **2019**, *333*, 190–195. [[CrossRef](#)]
52. Jiráťová, K.; Mikulová, J.; Klempa, J.; Grygar, T.; Bastl, Z.; Kovanda, F. Modification of Co-Mn-Al mixed oxide with potassium and its effect on deep oxidation of VOC. *Appl. Catal. A Gen.* **2009**, *361*, 106–116. [[CrossRef](#)]

Disclaimer/Publisher's Note: The statements, opinions and data contained in all publications are solely those of the individual author(s) and contributor(s) and not of MDPI and/or the editor(s). MDPI and/or the editor(s) disclaim responsibility for any injury to people or property resulting from any ideas, methods, instructions or products referred to in the content.